RESEARCH ARTICLE

ATMOSPHERIC ICE

Active sites in heterogeneous ice nucleation–the example of K-rich feldspars

Alexei Kiselev,[1]* Felix Bachmann,[1,2]† Philipp Pedevilla,[3] Stephen J. Cox,[3] Angelos Michaelides,[4] Dagmar Gerthsen,[2] Thomas Leisner[1,5]

Ice formation on aerosol particles is a process of crucial importance to Earth's climate and the environmental sciences, but it is not understood at the molecular level. This is partly because the nature of active sites, local surface features where ice growth commences, is still unclear. Here we report direct electron-microscopic observations of deposition growth of aligned ice crystals on feldspar, an atmospherically important component of mineral dust. Our molecular-scale computer simulations indicate that this alignment arises from the preferential nucleation of prismatic crystal planes of ice on high-energy (100) surface planes of feldspar. The microscopic patches of (100) surface, exposed at surface defects such as steps, cracks, and cavities, are thought to be responsible for the high ice nucleation efficacy of potassium (K)–feldspar particles.

The freezing of water is one of the most common everyday processes and hence is of relevance to an enormous number of technological and environmental phenomena. For example, ice formation is at the heart of precipitation formation in the majority of clouds, and therefore influences freshwater distribution. When water freezes, it does so in a heterogeneous process facilitated by the presence of foreign ice-nucleating (IN) particles. A wide variety of materials have been shown to be effective in promoting ice nucleation [see, e.g., Wilson *et al.* (*1*), Atkinson *et al.* (*2*), and Hiranuma *et al.* (*3*)], with mineral dust being the most abundant IN particle type in Earth's atmosphere (*4*, *5*). However, the IN efficacy of mineral dust (and other materials) varies by several orders of magnitude, and the question of what property (or combination of properties) is responsible for a particular mineral dust aerosol being a bad or good IN particle is debated (*4*, *6*–*10*).

Although there has been a considerable body of work aimed at understanding the structure of water and ice at interfaces, this has generally not provided detailed information about the mechanism of ice formation (*11*, *12*). In the absence of mechanistic insight, the IN efficacy of mineral dust solid particles is generally characterized by the surface density of IN active sites (*13*, *14*), an empirical parameter relating the apparent number of IN events to temperature and particle size (*15*). From previous experimental and modeling studies, several factors responsible for high IN efficacy of particles have been suggested (*4*, *16*–*20*): crystal lattice match allowing for epitaxial growth of ice (*21*–*26*), surface hydroxyl groups increasing the chemical affinity to ice (*17*, *19*, *27*–*31*), and surface defects (such as steps, cracks, and cavities) that locally enhance the density of adsorbed water molecules (*13*, *32*, *33*) or reduce their surface diffusivity (*17*, *34*). The importance of defects has been demonstrated in experiments where substrates with excellent lattice match to ice (such as silver iodide) could be made even more effective in nucleating ice through the introduction of surface morphological irregularities (*35*, *36*). However, recent molecular-scale simulations question the importance of lattice match and show that the connection with hydrophobicity can be extremely complex (*20*, *27*, *29*, *31*, *37*–*39*).

Owing to the lack of direct experimental evidence, it remains unclear which of the above factors plays a dominant role in regulating the IN properties of specific substrates. To better address this issue, we have performed an extensive set of experimental and modeling studies of ice nucleation on K-rich feldspar. This study focuses primarily on ice nucleation from water vapor (i.e., deposition mode nucleation) at cold temperatures (233 to 248 K). We have chosen feldspar because it has recently been identified as one of the most active atmospherically relevant IN minerals (*2*, *10*). The specific feldspar samples examined in our experiments were orthoclase from Michigan, USA (FSM) and microcline from the Mt. Maloso region, Malawi (FS04) [for more information on these samples, see recent work of Peckhaus *et al.* (*40*)]. On the basis of environmental scanning electron microscopy (ESEM) measurements, we find that ice crystals grow in a very specific manner, with the nucleation originating at defect sites of the substrate. From these high-resolution observations and molecular modeling, we conclude that the defective regions expose microscopic patches of (100) surfaces, and it is at these patches that ice grows along its prismatic face. Such (100) surfaces are not expressed as macroscopic surfaces of feldspar particles (i.e., they are not part of the equilibrium crystal shape of feldspar particles and are not produced by cleavage or environmental mechanical processing) but may be present microscopically at defective regions arising during natural weathering. This work therefore unravels the nature of the active sites in ice nucleation on feldspar and opens up a new paradigm for the mechanism of heterogeneous ice nucleation, wherein facets with relatively high surface free energy play a leading role.

ESEM observations of ice nucleation

K-Feldspar ($KAlSi_3O_8$) is a rock-forming framework silicate mineral. It has two crystallographic planes that lead to "perfect" (001) and "good" (010) cleavage (Fig. 1A). Even though a feldspar (001) surface is said to cleave perfectly, when prepared by mechanical splitting and examined in microscopic detail, it is far from being atomically smooth. It exposes a vast array of topographic features such as steps, cavities, and kinks (Fig. 2A and fig. S2). This surface complexity thus makes it ideal for studying IN active sites.

We observed the nucleation and growth of ice on feldspar samples mounted on a cooled specimen holder in an ESEM operating in an atmosphere of controlled relative humidity well below water saturation (see supplementary materials for details). In Fig. 2, we show results from an experiment involving a number of ice nucleation-evaporation cycles on the (001) face of the FSM sample at 233 K (movie S1). We find that ice invariably nucleates in the vicinity of defect sites such as steps, cracks, and inside cavities. This is particularly apparent by comparing Fig. 2, A and B, where in Fig. 2A, the sites of ice nucleation are indicated. Specifically, in Fig. 2A, the sites of ice nucleation are mapped onto the image of the bare feldspar specimen and are color-coded according to the time at which they appear. Nucleation sites cluster near the surface defects, and in every nucleation cycle, the first ice crystal (the largest hexagonal prism in Fig. 2B) always appeared in a cavity (red arrow in Fig. 2A; see also movie S4). Preferential nucleation of ice in the vicinity of defects occurs irrespective of the origin, the weathering procedure, or whether any chemical treatment was applied to the

[1]Atmospheric Aerosol Research Department, Institute for Meteorology and Climate Research (IMK-AAF), Karlsruhe Institute of Technology (KIT), Hermann-von-Helmholtz Platz 1, 76344 Eggenstein-Leopoldshafen, Germany. [2]Laboratory for Electron Microscopy (LEM), KIT, Engesserstrasse 7, 76131 Karlsruhe, Germany. [3]London Centre for Nanotechnology, Thomas Young Centre, and Department of Chemistry, University College London (UCL), 17-19 Gordon Street, London WC1H 0AH, UK. [4]London Centre for Nanotechnology, Thomas Young Centre, and Department of Physics and Astronomy, UCL, 17-19 Gordon Street, London WC1H 0AH, UK. [5]Institut für Umweltphysik, Universität Heidelberg, Im Neuenheimer Feld 229, Heidelberg, Germany.

***Corresponding author. Email: alexei.kiselev@kit.edu** †Present address: Max Planck Institute of Colloids and Interfaces, Am Mühlenberg 1, 14476 Potsdam, Germany.

specimens (for details, see the supplementary materials).

A key observation reported in this study is the almost perfect orientation of pristine ice crystals nucleating on K-rich feldspar throughout the atmospherically relevant temperature range from 248 to 233 K. This striking feature is already visible at the earliest stage of ice crystal growth (Fig. 2B) but shown in more detail in Fig. 3 and in movies S1 to S3. The orientation of ice crystals is identical with respect to (i) the inclination of the *c* axis of ice to the (001) face of feldspar and (ii) the rotational orientation of the ice crystals about their *c* axis (compare to Fig. 1B for illustration of the crystallographic planes and axes of hexagonal ice I_h). Of more than 300 individual ice crystals observed in this study, 80% have an identical orientation on the FSM specimen and 85% on the FS04 specimen. The average fraction of aligned crystals within each individual nucleation experiment was 90%. Most notably, the crystals exhibit the same orientation independent of whether they were nucleating on the (001) or (010) crystal faces of feldspar (see Fig. 3A and movie S3), implying that nucleation sites responsible for the orientation and alignment of the ice crystals are exposed in surface defects on both the (001) and (010) surfaces. This observation also suggests that contaminants on the surface (either chemical or biological in nature) are very unlikely to be responsible for ice nucleation, as they would have to coat the entire feldspar specimen and its different facets in a similar manner. In cases where multiple faces of the specimen were observed simultaneously, we could confirm that the nucleation on both the (001) and (010) surfaces occurred at very similar values of ice supersaturation (fig. S4).

From numerous experiments under different conditions (as outlined in the supplementary materials), we find that monocrystalline ice crystals grow in the same orientation when the following conditions are fulfilled: (i) The K-feldspar specimen has been aged, either naturally (exposed to laboratory air for at least a day) or in carbonated water; (ii) the cooling rate does not exceed 2 K/min (to ensure the diffusion-limited growth of ice crystal); and (iii) the onset temperature of ice nucleation is above 230 K. All three of these conditions are relevant for the deposition nucleation of ice on atmospheric mineral dust particles.

Under favorable observation conditions, the inclination of the ice crystals with respect to feldspar could be measured. In particular, as shown in Fig. 4, the (010) face of feldspar is lying in the image plane, and the *c* axis of the ice crystal is inclined by 116° with respect to the (001) feldspar face. This matches the angle β = 116.03° between the (001) and (100) crystallographic planes in ideal orthoclase feldspar (*41*) (Fig. 1A) and corresponds to perfect alignment of the *c* axes of feldspar and ice. In addition, all ice crystals showing this alignment have one of their prismatic axes (a_1...a_3; compare to Fig. 1B) parallel to the *b* axis of feldspar. These observations suggest that the orientation of the nucleated ice crystals is governed by the crystalline structure of the underlying feldspar sample. The observed match of the two lattice orientations can be explained by the ice crystal nucleating with its primary prism plane $(10\bar{1}0)$ on the (100) crystallographic plane of feldspar (see Fig. 1 for crystallographic planes of feldspar and ice).

Because of its high surface energy and associated fast growth rate from the melt, the (100) plane in feldspar rarely appears as a free-growing crystal face in natural macroscopic feldspar specimens (*41*). Tiny patches of this plane, however,

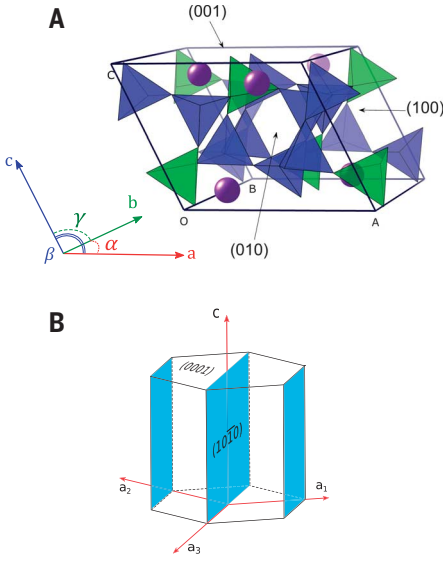

Fig. 1. Crystal structure and principal lattice planes in feldspar and ice. (**A**) K-feldspar (orthoclase): Unit cell angles are α = 90°, β = 116.03°, and γ = 90°; each Si^{4+} (blue) and each Al^{3+} (green) is located in the center of a tetrahedron with four oxygen atoms in its vertices (not shown). K^+ ions (violet spheres) occupy the framework voids and provide for the neutral electric charge of the bulk mineral structure. (**B**) Hexagonal lattice unit of ice I_h, showing the basal face (0001) and the family of primary prism planes $(10\bar{1}0)$ (translucent blue).

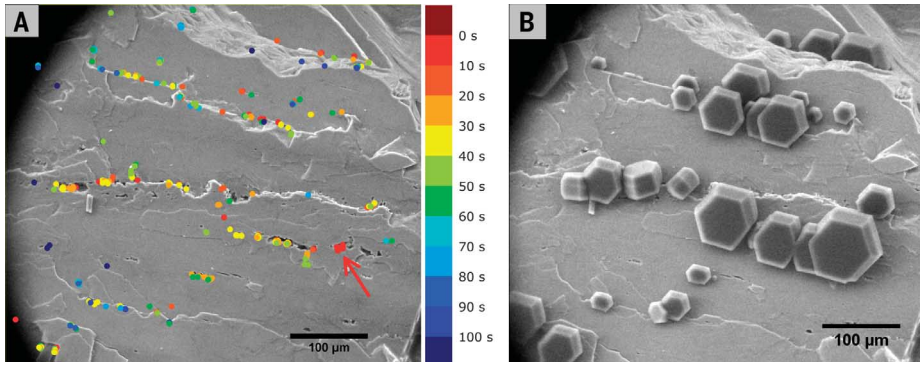

Fig. 2. Heterogeneous ice nucleation on (001) face of feldspar (FSM), weathered in carbonated water. (**A**) Nucleation sites of individual ice crystals in eight subsequent nucleation-evaporation cycles, plotted over the image of the bare feldspar face. The color code gives the time of nucleation (in seconds) with respect to the first detected crystal (the color scale bar is on the right). Preferential nucleation on steps and cavities is apparent. The red arrow shows the site of the first nucleation event that repeatedly occurs in all cycles. (**B**) Snapshot of the ice crystals nucleated at 233 K in the first nucleation-evaporation cycle.

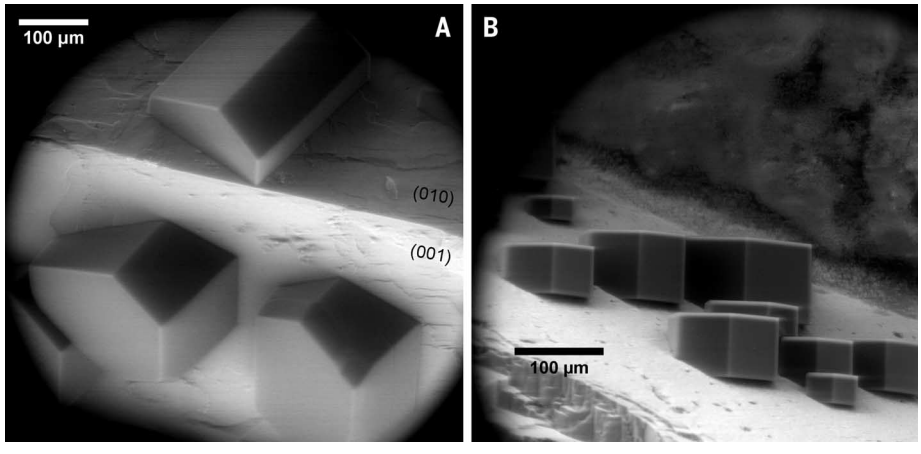

Fig. 3. Preferential orientation of ice crystals nucleated on the surface of weathered feldspar. (**A**) (010) and (001) surface of FSM at 241 K. (**B**) (001) surface of FS04 at 244 K, side view.

will appear at steps and in cavities on both cleavage faces as a result of mechanical fracture or weathering. Figure 4, A to E, provides direct evidence that this is indeed the case. These panels show a magnified image of a cavity in the (010) face of FSM with an ice crystal nucleating on one of the walls. The plane of the wall is aligned with the (100) crystal plane, as shown by the projection of the orthoclase unit cell (yellow) matching the crystal lattice of the specimen. Already at the earliest stage of growth (t < 2 s after nucleation, Fig. 4B), the ice crystal exhibits a preferential orientation that is consistent with the nucleation of its prism face on the (100) patch in feldspar. This orientation becomes obvious with further growth, when several other crystals appear on both faces of feldspar in the same orientation (t > 30 s, Fig. 4E). Figure 4F illustrates how the nucleation of ice from the $(10\bar{1}0)$ plane on a step with (100) orientation explains the identical orientation of ice crystals on both (001) and (010) faces of feldspar. The relative positions and orientation of ice crystals in Fig. 4F correspond to the case shown in Fig. 4E. The preferential ice orientation, combined with the fact that ice always seems to grow at defect sites where (100) patches may be exposed, suggests that these patches are the IN active sites.

At the early growth stage (t = 10 s, Fig. 4D), the crystal shape is not a hexagonal column but exhibits the true equilibrium growth habit of ice (*42*). In equilibrium, all crystallographic faces of ice (basal, prism, and pyramidal) grow with the same linear velocity. As the crystal becomes larger, the growth of basal and prism faces slows down and the pyramidal faces become less pronounced.

Atomistic simulations of feldspar-ice interface

Recently, some of us have shown on the basis of atomistic computer simulations that a stable ice-like structure can form on the most easily cleaved (001) surface of feldspar (*43*). In comparison to (001), the structure of the (100) surface of microcline is fairly complex, with a ~13 Å by 7 Å surface unit cell. In addition, in a wet environment, undercoordinated atoms arising from the cleavage of the surface will be terminated with hydroxyl groups [aluminol (Al-OH) and silanol (Si-OH)] (*41*, *44*–*46*). Given the complex structure of the feldspar (100) surface, it is not clear if ice can form stable structures on top of it. To address this issue, we carried out an extensive set of atomistic computer simulations in which we searched for stable ice-like structures at the feldspar (100) surface, based on the ClayFF force field (*47*) to represent feldspar and the SPC model to represent water (*48*). For comparison, we also searched for structures on the feldspar (010) and (110) surfaces, because the observed relative orientation of crystal habits of feldspar and ice can in principle be explained by ice growth from secondary prismatic planes on these surfaces (see supplementary materials for more details). A very broad range of ice structures was considered, and the main result is shown in Fig. 5, where we present an atomistic model of the feldspar (100)–ice interface. We do indeed find that the stable face of ice on the feldspar (100) surface is the primary prismatic plane $(10\bar{1}0)$ (with an adsorption energy of −0.58 eV per water molecule; for further details, see the supplementary materials). The prism plane is favored over the basal face because the rectangular symmetry of the former matches that of the underlying substrate fairly well, enabling a 3 × 1 array of prism face unit cells to fit within one unit cell of the feldspar (100) surface. Indeed, the fit between the prism face and the feldspar (100) surface is particularly good, with very little strain within the overlayer. This can be seen, for example, by measuring the median O-O (2.74 Å) distances and O-O-O (109.4°) angles within the ice overlayer. On average, these values are within 0.01 Å and 0.1° of the corresponding values in the simple point charge (SPC) model of bulk ice, with an equivalent computational setup. None of the other ice-like structures identified on the (100) surface or the other feldspar

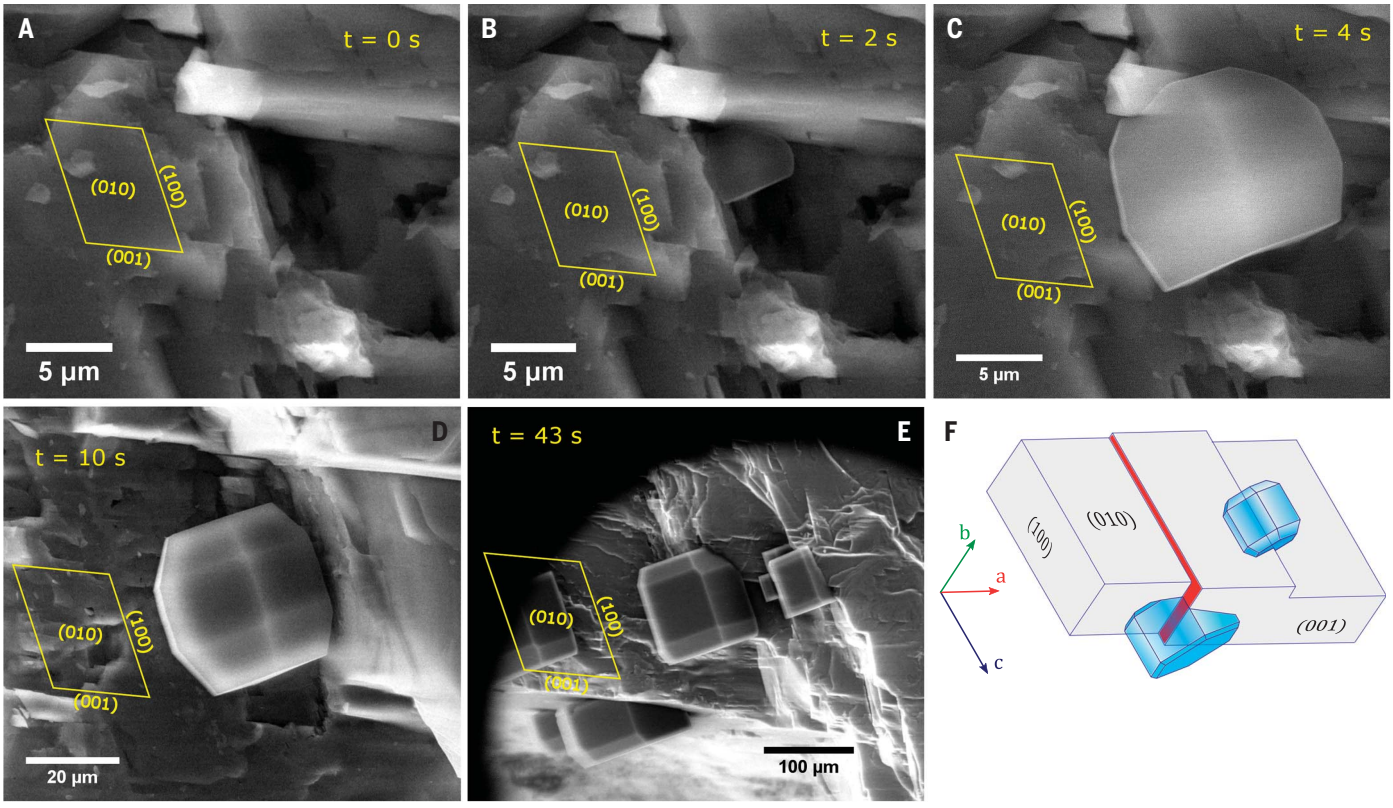

Fig. 4. Nucleation of an ice crystal on a patch with (100) orientation at 251 K. (**A** to **E**) An ice crystal nucleating on the inner wall of a cavity in the (010) face of the FSM specimen. The orientation of the wall visually corresponds to the (100) crystal plane of orthoclase. The relative orientation of crystal planes is shown in yellow, with (010) facing up. The specimen stage has not been moved between frames. (**F**) Schematic drawing of ice crystals nucleating from their $(01\bar{1}0)$ planes on the steps with (100) orientation [red filled surface and the hidden face of the step on the (010) face of feldspar; the relative position of ice crystals to each other and with respect to crystal faces of feldspar specimen corresponds to the case shown in (E)].

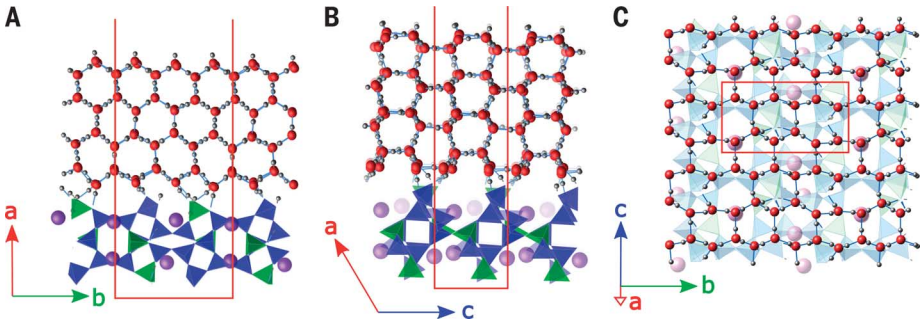

Fig. 5. The most stable structure of ice on feldspar (100) found in force field simulations. (**A** and **B**) Side views. (**C**) Top view. Ice I_h is attached with its primary prism plane ($10\bar{1}0$) to the (100) face of feldspar. Colors of tetrahedra are the same as in Fig. 1. Oxygen and hydrogen atoms in ice are shown in red and gray, respectively. In the top view (C), the feldspar underlying structure is shown in pale colors. The primitive feldspar (100) slab unit cell (orthogonal) used in the simulations is shown as the open red box, whereas the axes show the directional vectors of an ideal monoclinic feldspar unit cell.

surfaces yielded ice with as little strain as this feldspar (100)/ice ($10\bar{1}0$) interface.

Two aspects of the results are worth elaborating in more detail. First, contrary to the often implicitly made assumption that in the case of epitaxial growth, ice nucleates from the basal face, our results suggest that this does not happen on K-feldspar. Basal plane epitaxy was most often observed in the experiments with synthetic and natural substrates (*21*, *22*, *49*). However, nucleation of the prism plane on a substrate is not unknown (*21*). Several molecular dynamics studies have also found nucleation of a prism face aligned with the basal face of clay minerals (*19*, *31*).

Second, as shown in Fig. 5, the interaction between feldspar and water is indeed mediated by hydroxyl groups on the feldspar surface. The prism face grows directly on the hydroxylated (100) feldspar surface, in contrast to the predictions of ice growth on the (001) surface, where a non–ice-like layer mediates the structure between ice and the substrate (*43*). This suggests that surface OH groups play an important role in the ice nucleation process, by allowing ice-like structures to form even without an apparent epitaxial match. Thus, it is not surprising that affecting the OH arrangement by natural weathering or chemical treatment affects the ice nucleation process, as discussed further in the supplementary materials. The role of OH groups might provide a clue for understanding the observed strong variability of ice nucleation efficacies of various feldspars (*10*, *40*) because the natural variability of lattice constants, microtexture, heterogeneity of Al:Si ratio, and so forth will be reflected in the ordering of the surface hydroxyl groups, thus affecting the ability of feldspar dust particles to serve as IN particles.

We hypothesize that the affinity of feldspar (100) patches for ice, as described in this study, should be universal for both deposition and immersion modes of heterogeneous ice nucleation. In both regimes, the ability of the active site to reduce the energy of nucleus formation defines the ice nucleation efficiency of a substrate. In both regimes, the energy of the nucleus-substrate interface must be the same. What is different, however, is the flux of water molecules toward the critical nucleus and the surface tension of the nucleus, and therefore its size. We argue that the ability of (100) surface patch to bind a certain crystal plane of ice (prism) should be relevant in immersion freezing as well as in deposition ice nucleation, leading to acceleration of the nucleation rate. The ice nucleation onset conditions, as well as the observable features (habit and orientation of ice crystals), will, of course, be different for different nucleation modes.

Conclusions

In this study, we have experimentally identified the IN active sites on the surface of K-rich feldspar as the surface patches with (100) crystallographic orientation. These patches occur exclusively at surface features like steps, cracks, and cavities that arise during fracturing processes (such as grinding or mechanical weathering). The preferential nucleation of ice on the defects is dominated by the presence of these patches. This finding will help to characterize the IN properties of natural mineral dust aerosol particles, which almost universally contain feldspar. The feldspar particles with the highest density of specific crystal planes exposed in the surface defects should constitute the most efficient IN particles. Moreover, aided by atomistic computer simulations, we showed that on these patches, hydroxyl groups mediate the interaction between ice and feldspar. These observations constitute direct identification of an IN surface site on an inorganic substrate at the molecular level. The nucleation of nonbasal faces of ice on surfaces with relatively high surface free energy, which are not expressed as dominant surface facets, could be relevant to ice formation on other mineral dusts and substrates.

REFERENCES AND NOTES

1. T. W. Wilson *et al.*, *Nature* **525**, 234–238 (2015).
2. J. D. Atkinson *et al.*, *Nature* **498**, 355–358 (2013).
3. N. Hiranuma *et al.*, *Nat. Geosci.* **8**, 273–277 (2015).
4. M. A. Freedman, *J. Phys. Chem. Lett.* **6**, 3850–3858 (2015).
5. N. Hiranuma *et al.*, *Atmos. Chem. Phys.* **14**, 13145–13158 (2014).
6. C. Hoose, O. Möhler, *Atmos. Chem. Phys.* **12**, 9817–9854 (2012).
7. B. J. Murray, D. O'Sullivan, J. D. Atkinson, M. E. Webb, *Chem. Soc. Rev.* **41**, 6519–6554 (2012).
8. J. D. Yakobi-Hancock, L. A. Ladino, J. P. D. Abbatt, *Atmos. Chem. Phys.* **13**, 11175–11185 (2013).
9. G. P. Schill, K. Genareau, M. A. Tolbert, *Atmos. Chem. Phys.* **15**, 7523–7536 (2015).
10. A. D. Harrison *et al.*, *Atmos. Chem. Phys.* **16**, 10927–10940 (2016).
11. A. Hodgson, S. Haq, *Surf. Sci. Rep.* **64**, 381–451 (2009).
12. J. Carrasco, A. Hodgson, A. Michaelides, *Nat. Mater.* **11**, 667–674 (2012).
13. N. H. Fletcher, *J. Atmos. Sci.* **26**, 1266–1271 (1969).
14. N. H. Fletcher, *Aust. J. Phys.* **13**, 408–418 (1960).
15. P. J. Connolly *et al.*, *Atmos. Chem. Phys.* **9**, 2805–2824 (2009).
16. W. Cantrell, A. Heymsfield, *Bull. Am. Meteorol. Soc.* **86**, 795–807 (2005).
17. H. R. Pruppacher, J. D. Klett, *Microphysics of Clouds and Precipitation* (Kluwer Academic Publishers, ed. 2, 2004).
18. G. Vali, *Molecules* **1999**, 1–22 (1999).
19. S. J. Cox, Z. Raza, S. M. Kathmann, B. Slater, A. Michaelides, *Faraday Discuss.* **167**, 389–403 (2013).
20. M. Fitzner, G. C. Sosso, S. J. Cox, A. Michaelides, *J. Am. Chem. Soc.* **137**, 13658–13669 (2015).
21. G. W. Bryant, J. Hallett, B. J. Mason, *J. Phys. Chem. Solids* **12**, 189–195 (1960).
22. J. L. Caslavsky, K. Vedam, *J. Appl. Phys.* **42**, 516–520 (1971).
23. N. Cho, J. Hallett, *J. Cryst. Growth* **69**, 317–324 (1984).
24. T. Kobayashi, *Contrib. from Inst. Low Temp. Sci.* **A20**, 1–22 (1965).
25. B. Vonnegut, *J. Appl. Phys.* **18**, 593–595 (1947).
26. D. Turnbull, B. Vonnegut, *Ind. Eng. Chem.* **44**, 1292–1298 (1952).
27. T. Croteau, A. K. Bertram, G. N. Patey, *J. Phys. Chem. A* **112**, 10708–10712 (2008).
28. T. Croteau, A. K. Bertram, G. N. Patey, *J. Phys. Chem. A* **113**, 7826–7833 (2009).
29. X. L. Hu, A. Michaelides, *Surf. Sci.* **601**, 5378–5381 (2007).
30. X. L. Hu, A. Michaelides, *Surf. Sci.* **602**, 960–974 (2008).
31. S. A. Zielke, A. K. Bertram, G. N. Patey, *J. Phys. Chem. B* **120**, 1726–1734 (2016).
32. H. K. Christenson, *CrystEngComm* **15**, 2030 (2013).
33. C. Marcolli, *Atmos. Chem. Phys.* **14**, 2071–2104 (2014).
34. B. Federer, *Z. Angew. Math. Phys.* **19**, 637–665 (1968).
35. J. Hallett, S. K. Shrivastava, *J. Rech. Atmos.* **5**, 223–236 (1973).
36. B. J. Anderson, J. Hallett, *J. Atmos. Sci.* **33**, 822–832 (1976).
37. S. J. Cox, S. M. Kathmann, J. A. Purton, M. J. Gillan, A. Michaelides, *Phys. Chem. Chem. Phys.* **14**, 7944–7949 (2012).
38. L. Lupi, V. Molinero, *J. Phys. Chem. A* **118**, 7330–7337 (2014).
39. L. Lupi, A. Hudait, V. Molinero, *J. Am. Chem. Soc.* **136**, 3156–3164 (2014).
40. A. Peckhaus, A. Kiselev, T. Hiron, M. Ebert, T. Leisner, *Atmos. Chem. Phys.* **16**, 11477–11496 (2016).
41. J. V. Smith, *Feldspar Minerals 2 Chemical and Textural Properties* (Springer, Berlin, Heidelberg, ed. 1, 1974).
42. K. G. Libbrecht, *Proc. R. Soc. London* **49**, 323–343 (2012).
43. P. Pedevilla, S. J. Cox, B. Slater, A. Michaelides, *J. Phys. Chem. C* **120**, 6704–6713 (2016).
44. I. Parsons, Ed., *Feldspars and Their Reactions* (Kluwer Academic Publishers, Series C, 1994), vol. 421.
45. J. V. Smith, *Proc. Natl. Acad. Sci. U.S.A.* **95**, 3366–3369 (1998).
46. H. Behrens, *Mineral. Mag.* **59**, 15–24 (1995).
47. R. T. Cygan, J.-J. Liang, A. G. Kalinichev, *J. Phys. Chem. B* **108**, 1255–1266 (2004).
48. H. J. C. Berendsen, J. P. M. Postma, W. F. van Gunsteren, J. Hermans, in *Intermolecular Forces*, B. Pullman, Ed. (Springer Netherlands, 1981), pp. 331–342.
49. N. Fukuta, B. Mason, *J. Phys. Chem. Solids* **24**, 715–718 (1963).

ACKNOWLEDGMENTS

The preparation and x-ray diffraction characterization of feldspar samples at the Institute of Applied Geosciences of TU Darmstadt (M. Ebert) as a part of cooperation within the Deutsche Forschungsgemeinschaft (DFG)–funded research unit INUIT (DFG-FOR-1525-6343) is greatly acknowledged. This work was also partly supported by KIT Startup Budget 2011

(2066992441-Start-Up-Eisbildung-ESEM GG 507). A.K and F.B. thank V. Zibat (KIT LEM) and J. Nadolny (KIT IMK-AAF) for technical and programming support. A.M. is supported by the European Research Council under the European Union's Seventh Framework Programme (FP/2007-2013)–European Research Council Grant Agreement no. 616121 (HeteroIce project). A.M. is also supported by the Royal Society through a Royal Society Wolfson Research Merit Award. P.P. and A.M. are grateful for computational resources provided by the Materials Chemistry Consortium through the Engineering and Physical Sciences Research Council grant no. EP/L000202, UCL Research Computing, and the London Centre for Nanotechnology. A.K. and T.L. are supported by the Helmholtz Association under Atmosphere and Climate Programme (ATMO). D.G. and F.B. were supported by the Karlsruhe Institute of Technology. The experimental and computational data sets used in this work are available as supplementary materials.

SUPPLEMENTARY MATERIALS

www.sciencemag.org/content/355/6323/367/suppl/DC1
Author Contributions
Materials and Methods
Supplementary Text
Figs. S1 to S9
Table S1
Movies S1 to S4
References (*50*–*63*)
GROMACS Structure File of Ice on Feldspar (100)
Data Files S1 and S2

13 August 2016; accepted 23 November 2016
Published online 8 December 2016
10.1126/science.aai8034

Active sites in heterogeneous ice nucleation—the example of K-rich feldspars

Alexei Kiselev, Felix Bachmann, Philipp Pedevilla, Stephen J. Cox, Angelos Michaelides, Dagmar Gerthsen and Thomas Leisner

Science **355** (6323), 367-371.
DOI: 10.1126/science.aai8034originally published online December 8, 2016

From dust to ice

How does ice form on the surfaces of aerosol particles? The process is important for climate and atmospheric properties but poorly understood at the molecular level, in part because the nature of the sites where ice growth begins is unclear. Kiselev *et al.* used electron microscopy and computer simulations to study the deposition of aligned ice crystals on feldspar, a major component of mineral dust (see the Perspective by Murray). Surface defects of the feldspar were responsible for its high ice-nucleation efficiency.

Science, this issue p. 367; see also p. 346